

This un-edited manuscript has been accepted for publication in Biophysical Journal and is freely available on BioFast at <http://www.biophysj.org>. The final copyedited version of the paper may be found at <http://www.biophysj.org>.

A Kinetic Model of Single and Clustered IP₃ Receptors in the Absence of Ca²⁺ Feedback

Jianwei Shuai¹, John E. Pearson², J. Kevin Foskett³, Don-On Daniel Mak³
and Ian Parker¹

¹Department of Neurobiology and Behavior, University of California, Irvine, CA 92697, USA

²Theoretical Biology and Biophysics, T-10 K710, Los Alamos National Laboratory, Los Alamos, NM 87545, USA

³Department of Physiology, University of Pennsylvania, School of Medicine, Philadelphia, PA 19104, USA

Running title: Modeling single and clustered IP₃Rs

Address correspondence to:

Dr. Jianwei Shuai
Department of Neurobiology & Behavior
University of California, Irvine, CA 92697-4550
Tel.: 949 824 7833
Fax: 949 824 2447
Email: shuaij@uci.edu

Keywords: Calcium / IP₃ / Puffs / Channel / Patch Clamp / Stochastic Dynamics

ABSTRACT

Ca^{2+} liberation through inositol 1,4,5-trisphosphate receptor/channels generates complex patterns of spatio-temporal cellular Ca^{2+} signals owing to the biphasic modulation of channel gating by Ca^{2+} itself. These processes have been extensively studied in *Xenopus* oocytes, where imaging studies have revealed local Ca^{2+} signals ('puffs') arising from clusters of IP_3R , and patch-clamp studies on isolated oocyte nuclei have yielded extensive data on IP_3R gating kinetics. To bridge these two levels of experimental data we developed an IP_3R model, and applied stochastic simulation and transition matrix theory to predict the behavior of individual and clustered IP_3R channels. The channel model consists of four identical, independent subunits, each of which has an IP_3 -binding site, together with one activating and one inactivating Ca^{2+} binding site. The channel opens when at least three subunits undergo a conformational change to an 'active' state after binding IP_3 and Ca^{2+} . The model successfully reproduces patch-clamp data; including the dependence of open probability, mean open duration and mean close duration on $[\text{IP}_3]$ and $[\text{Ca}^{2+}]$. Notably, the bi-exponential distribution of open time duration and the dependence of mean open time on $[\text{Ca}^{2+}]$ are explained by populations of openings involving either three or four active subunits. As a first step toward applying the single IP_3R model to describe cellular responses we then simulated measurements of puff latency following step increases of $[\text{IP}_3]$. Assuming that stochastic opening of a single IP_3R at basal cytosolic $[\text{Ca}^{2+}]$ and any given $[\text{IP}_3]$ has a high probability of rapidly triggering neighboring channels by calcium-induced calcium release to evoke a puff, optimal correspondence with experimental data of puff latencies following photorelease of IP_3 was obtained assuming that the cluster contains 40 - 70 IP_3Rs totally.

INTRODUCTION

The inositol 1,4,5-trisphosphate receptor (IP₃R) acts as a Ca²⁺ release channel to liberate Ca²⁺ ions from the endoplasmic reticulum (ER) into the cytosol [1]. Structurally, the IP₃R is a large (~30 nm diameter) homomeric tetramer of four subunits forming a single ion-conducting channel [2]. Each subunit is composed of three functionally different domains, including a large cytoplasmic region of amino-terminal IP₃-binding domain, a carboxy-terminal channel-forming domain, and a middle coupling modulatory and transducing domain [3, 4]. Opening of the channel requires the binding of the second messenger inositol 1,4,5-trisphosphate (IP₃), which is generated in the cytoplasm in response to the binding of extracellular ligands to plasma membrane receptors. Moreover, gating of the IP₃R is biphasically modulated by Ca²⁺ ions, such that small elevations of cytosolic [Ca²⁺] promote channel opening whereas higher [Ca²⁺] results in inactivation [5]. This Ca²⁺ feedback underlies a process of Ca²⁺-induced Ca²⁺ release (CICR), resulting in regenerative liberation of Ca²⁺ that may either remain restricted to a cluster of IP₃R to generate a localized Ca²⁺ puff [6], or may propagate as a saltatory wave across numerous puff sites by successive cycles of Ca²⁺ diffusion and CICR.

To elucidate the complex spatio-temporal patterns of Ca²⁺ signals generated by the IP₃ pathway we thus need to understand the functioning of IP₃Rs at the single molecule level, the spatial arrangement of these receptors in the cell, and their functional interactions via Ca²⁺ diffusion and CICR. The *Xenopus* oocyte provides a favorable cell system with which to investigate these topics, by virtue of the wealth of experimental data available regarding both the imaging of IP₃-evoked Ca²⁺ signals in the intact cell [6-8], and patch-clamp recordings of single IP₃R in the outer membrane of isolated oocyte nuclei [9-12]. To bridge these two levels of experimental data we developed an IP₃R model, and used both transition matrix theory and stochastic simulation to predict the behavior of individual and clustered channels.

Models of the IP₃R play a central role not only for the understanding channel kinetics, but also as building blocks for constructing larger-scale models of cellular Ca²⁺ signaling. Several IP₃R models [13-19] have been developed to describe experimental data obtained from IP₃R reconstituted in bilayers membrane, with the DeYoung–Keizer model [14] in particular being widely applied. However, there are significant differences in behavior of the reconstituted IP₃R versus that of IP₃R in their native environment of the nuclear envelope, and only a few models have incorporated IP₃R data obtained on nuclei membrane. Among these, an allosteric four-plus-two-conformation model was considered by Mak et al [11]. That model postulates that each of the four IP₃R monomers has one IP₃-binding site and three different functional Ca²⁺-binding sites on the cytoplasmic side of the channel. Another model was developed by Baran [20], consisting of one activation module and one inhibition module, both allosterically operated by Ca²⁺, IP₃, and ATP, together with one adaptation module, driven by IP₃ and Ca²⁺. However,

these two models can predict only the steady-state gating properties, and not the kinetics of individual channel openings and closings.

Thus, there is still a lack of a model that can realistically simulate the kinetic behavior of IP₃R under physiological conditions in the *Xenopus* oocyte. Our aim was to develop a dynamic IP₃R model that successfully reproduces data obtained from patch-clamp of nuclear IP₃R, and that is sufficiently simple and computationally tractable to applied in future studies simulating the interactions of numerous IP₃R coupled in a cellular environment by Ca²⁺ diffusion and CICR. The channel model consists of four identical, independent subunits, each of which has an IP₃-binding site, together with one activating and one inactivating Ca²⁺ binding site. A feature of the model is that channel opening may occur if either 3 or 4 of the subunits of the tetramer are in an 'activated' state (binding both IP₃ and activating Ca²⁺ ion, but not inhibitory Ca²⁺ ion), and we show how this characteristic can account for the observed bi-exponential distribution of open times and the dependence of mean open time on [Ca²⁺]. Moreover, we extend our IP₃R channel model to the cellular level, by simulating the latencies of puffs following step increases of IP₃, on the assumption that the stochastic opening of a single IP₃R within a cluster rapidly evokes CICR from neighboring channels with high probability to generate a puff. On this basis, we predict that puff sites contain a total of 40 – 70 IP₃Rs.

MODEL

A schematic picture of the IP₃R model is shown in Fig. 1. which, from structural studies [2], comprises four identical and independent subunits. Based on experimental observations that the channel open probability is a bell-shaped function of [Ca²⁺] [5, 10, 15], we consider two independent Ca²⁺ binding sites for each subunit; i.e., an activating binding site and an inhibitory site. Consistent with the molecular structure of the IP₃R [3, 4] and concordant with most previous IP₃R models, we also assume a single IP₃ binding site in each subunit. The state of each subunit is denoted as $(i j k)$, where the index i represents the IP₃ binding site, j the activating Ca²⁺ binding site, and k the inhibitory Ca²⁺ binding site. An occupied site is represented as 1, and a non-occupied site as 0.

The model further includes a conformational change whereby a subunit in the (110) state (one IP₃ and one activating Ca²⁺ bound) is 'inactive', and must transition to an 'active' (A) state before it can contribute to channel opening. This conformational step is analogous to the well-characterized behaviour of nicotinic acetylcholine receptors [21], and further implies that the active state is 'locked' with respect to agonist binding and dissociation. Observations of ligand-independent flickerings of the IP₃R channel to the closed state [11] are consistent with such a conformational change, and the lack of effect of changes in Ca²⁺ concentration on gating of already open IP₃R channels [22] support the notion that active subunits are locked with respect to ligand binding.

We also assume that the channel is open when either three or four subunits are in active state. This assumption has previously been applied in some IP₃R models [23], and we show here that it can explain the dependence of channel open time on ligand concentration. Although some multimeric channels show distinct conductance levels associated with ligand binding to differing numbers of subunits [24], the *Xenopus* oocyte IP₃R displays only a single major conductance level [11, 12], so we distinguish only a single open state irrespective of whether 3 or 4 subunits are active.

Each subunit in the model has 9 states, with transitions governed by second-order rate constants (a_i with $i > 0$) for binding processes, first-order rate constants (b_i with $i > 0$) for unbinding process, and constant transition rates (a_0 and b_0) applied between the active A-state and the inactive (110) state (Fig. 1). Parameter values used in the model are listed in Table 1. Values for dissociation constants were chosen on the basis of optimal fit to steady-state experimental data from patch-clamped oocyte nuclear IP₃R (Fig. 2). For all the binding/unbinding loops given in Fig. 1, the thermodynamic constraint of detailed balance requires that $K_1 K_2 = K_3 K_4$ for reaction dissociation constants. The conformation rate changes a_0 and b_0 between the (110) and active states of the subunits were chosen to give a maximum channel open probability of about 0.84, as observed experimentally for *Xenopus* oocyte nuclei [10, 11]. The rate constant for IP₃ binding was based on experimental measurements of first opening latencies of 0.35 and

0.5 s for IP₃R channels in Sf9 cell nuclei at [Ca²⁺]=2 μM following step increases in [IP₃] from 0 to 10 and 100 μM, respectively (K. Foskett and D.O. Mak; unpublished data). Model simulations of single channel latencies provided a good fit, with predicted corresponding mean latencies of 0.34 and 0.4 s. Rate constants for Ca²⁺ binding were estimated by iterative fitting of model predictions to published data of *Xenopus* oocyte IP₃R open and closed time distributions [10, 11].

We explored the behaviour of the IP₃R model using both deterministic, matrix transition analysis and stochastic simulation. The deterministic approach provides a rigorous analytical solution of statistical channel behavior, but cannot reveal the trajectory of openings and closings of an individual IP₃R. Because we wish to use the model as a building block to explore the contribution of stochastic single-channel behaviour to cellular Ca²⁺ signaling we also performed stochastic simulations; an approach that has the further advantage of providing a more intuitive insight into the channel behavior.

Deterministic analysis of the IP₃R model

The probability of subunits in state (*ijk*) or (A) is denoted by P_{ijk} or P_A with $P_A + \sum P_{ijk} = 1$. By the mass action kinetics, the equations describing the subunit dynamics are written:

$$\frac{dP}{dt} = PQ \quad (1)$$

where Q is the generator matrix [25] of transition rates and P is the vector of probability of subunits. The open probability for an IP₃R is then given by:

$$P_o = P_A^4 + 4P_A^3(1 - P_A) \quad (2)$$

Mathematically, the equilibrium state is defined by $dP/dt = 0$. The equilibrium vector w satisfies $wQ = 0$. Detailed balance is imposed so we can solve for w by inspection [26]. This is done by calculating all probabilities in terms of their probability relative to state (000). These unnormalized probabilities are denoted q_{ijk} with $q_{0000} = 1$. Then

$$w_{ijk} = \frac{q_{ijk}}{Z} \quad (3)$$

where each component (q_{ijk} / Z) gives the equilibrium probability for state (*ijk*). Z is the normalization factor defined by $Z = q_A + \sum q_{ijk}$. The equilibrium probability (q_{ijk}) of state (*ijk*) relative to that of state (000) is just the product of forward to backwards rates along any path connecting (000) to (*ijk*). Thus we can write

$$q_A = \frac{[IP_3] \cdot [Ca^{2+}]}{K_1 K_5} \times \frac{a_0}{b_0} \quad (4)$$

and

$$Z = \left(1 + \frac{[Ca^{2+}]}{K_4}\right) \left(1 + \frac{[Ca^{2+}]}{K_5}\right) + \frac{[IP_3]}{K_1} \left(1 + \frac{[Ca^{2+}]}{K_2}\right) \left(1 + \frac{[Ca^{2+}]}{K_5}\right) + q_A$$

(5)

The equilibrium probability for the subunit active state is given by:

$$w_A = \frac{q_A}{Z} = \frac{[\text{IP}_3] \cdot [\text{Ca}^{2+}]}{K_1 K_5} \times \frac{a_0}{b_0} \times \frac{1}{Z} \quad (6)$$

Since the channel is open if either 3 or 4 subunits are active, the equilibrium open probability is a sum of contribution from three and four active subunits: $p_3 = 4w_A^3(1-w_A)$ and $p_4 = w_A^4$. Thus the open probability at the equilibrium state for an IP₃R channel is:

$$P_o = w_A^4 + 4w_A^3(1-w_A) \quad (7)$$

Because channel states (A, A, A, not-A) are only open states that connect to closed channel states by any one of three A-states changing to the closed state 110 with rate b_0 , we can directly write the equilibrium probability flux between open and closed states as follows:

$$J = 3b_0 p_3 \quad (8)$$

The mean open and closed times are given by:

$$\begin{aligned} \tau_o &= \frac{P_o}{J} = \frac{1}{3b_0} \times \frac{P_o}{p_3} = \frac{1}{3b_0} \times \left(1 + \frac{p_4}{p_3}\right) \\ \tau_c &= \frac{1-P_o}{J} = \frac{1}{3b_0} \times \frac{1-P_o}{p_3} \end{aligned} \quad (9)$$

Eq. (9) implies that the channel mean open time varies even though the subunit mean active time is fixed. τ_o has a limiting minimum value of $1/(3b_0)$ and increases as p_4/p_3 increases. This is to be expected since the channel is open if either 3 or 4 subunits are active but closes only when there are precisely 3 active subunits.

Deterministic solutions presented in Fig. 2 (showing the open probability P_o , mean open time τ_o and the mean close time τ_c as a function of constant Ca^{2+} concentration at different IP₃) were obtained using Eqs. 7 and 9. Furthermore, we applied the transition matrix theory to predict the open and closed time distributions of the channel in steady state and the distributions of the first-opening latency of individual and clustered IP₃Rs responding to step IP₃ stimulus. The analytic deductions employed to obtain those results will be described in detail in a separate paper (Shuai, Parker & Pearson; unpublished).

Stochastic simulation of the IP₃R model

We simulated the stochastic dynamics of this 9-state subunit channel model by a Markov process [27, 28], updating the state of the system at small time steps dt . For example, a channel subunit in the (110) state at time t could transition to states (010), (100), (111), or to the active A-state at the next time step $t + dt$ with respective transition probabilities of $b_1 dt$, $b_5 dt$, $a_2 [\text{Ca}^{2+}] \cdot dt$, or $a_0 dt$; otherwise remain in the same state. Random numbers homogeneously distributed in [0,1] were generated at each time step and compared with these transition probabilities in order to determine the state of the

channel subunit at the next time step. The IP₃R channel is open when 3 or 4 subunits are in the A-state. A time step $dt = 10 \mu\text{s}$ was generally used, being much shorter than mean channel open or closed times. The results were not appreciably different when dt was altered between 0.1 - 50 μs - and the close correspondence obtained with results of the deterministic analysis further validates the simulation method.

RESULTS

Steady-State IP₃R Dynamics

In this section, we describe the behavior of the single IP₃R model under steady-state conditions of given [IP₃] and [Ca²⁺], and demonstrate that our model successfully reproduces the experimental data obtained from patch-clamped IP₃R on the *Xenopus* oocyte nuclear membrane [9-12].

An example of stochastic channel gating

Fig. 2A illustrates stochastic channel gating, and the corresponding subunit states under conditions ([IP₃] = 10 μM and [Ca²⁺] = 0.2 μM) that result in a mean open probability (P_o) of about 0.4. Because the channel opens when either three or four subunits are active, we can distinguish two different types of channel open state: A3-only openings and A4-related openings. We define A3-only openings as those involving only three simultaneously active subunits throughout the duration of the opening, whereas A4-related openings involve at least one occurrence of all four subunits being active (e.g. openings marked by arrows in Fig. 2A).

Dependence of open probability on [IP₃] and [Ca²⁺]

The filled symbols in Fig. 2B show experimental measurements from oocyte nuclei of the dependence of IP₃R channel open probability (P_o) as a function of cytosolic [Ca²⁺] for different concentrations of IP₃ [10, 11]. The data follow the well-known 'bell-shape' distribution, with increasing concentrations of IP₃ producing a rightward shift in the Ca²⁺ concentration required for maximal P_o , and with the maximal P_o increasing steeply for IP₃ concentrations between 10 and 33 nM. These experimental observations are fit reasonably well by our IP₃R model, as shown in Fig. 2B by results obtained from both deterministic analysis (solid curves) and stochastic simulation (open symbols). An exception is that the model predicts a less steep dependence of P_o at low values of [IP₃R] than was experimentally observed.

A maximal $P_o = 0.84$ was achieved with the model under optimal conditions ([IP₃] > 0.5 μM and [Ca²⁺] ~ 3 μM). This corresponds well with measurements from IP₃R on the *Xenopus* oocyte nucleus [10, 11], but is much greater than that ($P_o \sim 0.2$) observed for cerebellar IP₃R reconstituted in lipid bilayers [5]. Concentrations of IP₃ greater than about 0.5 μM are already saturating, as expected from the relatively high binding affinity ($K_1 = 0.0036$ μM) in the model.

Mean open and close time

The mean open (τ_o) and closed (τ_c) times of the IP₃R channel are plotted, respectively, in Figs 2C,D as functions of Ca²⁺ and IP₃ concentrations for the deterministic (solid curves) and stochastic (open symbols) versions of the IP₃R model, together with experimental data (filled symbols) from oocyte nuclear receptors at [IP₃] = 10 μM [10].

It is evident that the dependence of P_o upon $[Ca^{2+}]$ and $[IP_3]$ described in Fig. 2B arises primarily through correspondingly large changes in τ_c , and the model results with $10 \mu M$ IP_3 fit well to the experimental observations. Additionally, although subject to appreciable scatter, the patch-clamp data, also reveal a modest (2-3 fold) increase in τ_o associated with increasing P_o [10]. This behaviour is reproduced by our model (Fig. 2C).

Variation of mean open time on $[IP_3]$ and $[Ca^{2+}]$

At first sight the dependence of predicted τ_o on ligand concentrations (Fig. 2C) appears unexpected, given that the transition rate b_0 from the active A-state to the close state (1110) of each subunit is a fixed value, resulting in a constant active dwell time of $1/b_0$ for each subunit. Theory (Eqs. 9) indicates that mean open time τ_o varies with $[Ca^{2+}]$ and $[IP_3]$ because the probability for being in the gateway states in which 3 subunits are active varies with respect to being in the single state with 4 active subunits. Indeed the theory is in solid accord with the experimental data in which the mean open time varies by about a factor of two. The variation in τ_o is given by the factor $1 + p_3/p_4 = 1 + w_A/(4(1 - w_A))$ (see Eqs.9). The IP_3R is observed to have a maximum P_o of about 0.84. To within a few percent P_o takes on its maximum value of 0.84 when w_A is about 0.8. This occurs when $p_3 = p_4$. Thus theory predicts that the channel mean open time varies by a factor of two in accord with observation. To further illustrate this point we analyzed the results of stochastic simulations, and show below that the variation in mean open time results because there are two populations of channel open states, involving only 3 active subunits, or at least one occurrence of 4 active subunits.

We first determined the mean open times associated with each of these conformations. Fig. 3A shows that mean open times for A3-only openings (T_3) and for A4-related openings (T_4) change only slightly as a function of $[Ca^{2+}]$ at $[IP_3] = 10 \mu M$, with respective values of about 2.6 – 4.2 and 14.5 – 15.5 ms. The mean open time T_{A3} can be intuitively understood because the channel will close when any one of the 3 active subunits becomes inactive, so that $T_{A3} \sim 1/(3b_0) \sim 4$ ms.

Because the mean dwell times of A3- and A4-related openings have only a slight ligand dependence, the change in mean channel open time with ligand concentration must, therefore, involve also a change in proportion of A3- and A4-related events. For example, with $[Ca^{2+}]$ at an optimal value of about $3 \mu M$, each subunit will have a high probability of being in the active state, thereby increasing the probability of finding 4 active subunits; whereas at lower $[Ca^{2+}]$ the probability of subunits having Ca^{2+} bound to the activating site is lower, and at higher $[Ca^{2+}]$ there is an increasing chance of subunits becoming inhibited. Thus, the probability for A4-related openings P_{A4} first increases and then decreases with increasing $[Ca^{2+}]$, and the probability P_{A3} for A3-only openings correspondingly follows an inverse relationship (Fig. 3B).

The mean open time of the channel expressed as

$$\tau_o = P_{A3}T_{A3} + P_{A4}T_{A4} \quad (10)$$

therefore varies as a function of C and I . At very low and high $[\text{Ca}^{2+}]$, the mean open time τ_o derives almost entirely from the A3-only open state, giving a value of $\tau_o \approx 4$ ms. At the optimal value of $[\text{Ca}^{2+}] \sim 3 \mu\text{M}$, $P_{A3} \approx P_{A4} = 0.5$ (Fig. 3B), so that $\tau_o \approx 0.5 \cdot (T_{A3} + T_{A4}) \approx 9$ ms.

Open and closed time distributions

Patch-clamp experimental data show that open channel dwell times follow a bi-exponential distribution, with time constants of about 4 ms and 20 ms [12]. This behavior is predicted also by our model with stochastic simulation and deterministic theory, where the open time distributions at various $[\text{Ca}^{2+}]$ are approximated by a sum of two exponentials (Fig. 4A). These two exponential components can be considered as arising from A3-only and A4-related openings. For example, the distributions of A3-only and A4-related open dwell times are plotted in Fig. 4B for $[\text{Ca}^{2+}] = 2 \mu\text{M}$ and $[\text{IP}_3] = 10 \mu\text{M}$. The distribution of A3-only openings is mono-exponential, with a time constant of ~ 4 ms, and the distribution of A4-related openings approximates an exponential with time constant ~ 12 ms for openings > 10 ms. For various $[\text{Ca}^{2+}]$ at $[\text{IP}_3] = 10 \mu\text{M}$, time constants of A3-only and A4-related exponential open distribution are about 3 - 5 and 9 - 14 ms, respectively.

Patch-clamp experimental data show that the IP_3R channel has at least two closed states, with the time constants about 1 ms and 10 ms, as well as a long closed kinetic state with time constant of the order of seconds [12]. Our model predicts also a rich kinetic behavior for closed dwell times. Three examples of close time distributions are plotted in Fig. 5A for $[\text{Ca}^{2+}] = 0.2, 2.0$ and $200 \mu\text{M}$ at $[\text{IP}_3] = 10 \mu\text{M}$. For $[\text{Ca}^{2+}] = 0.2 \mu\text{M}$ (the upper panel in Fig. 5A), three exponential components can be clearly distinguished at regions $\tau_c < 10$ ms, $20 < \tau_c < 400$ ms, and $\tau_c > 450$ ms with time constants of 1, 25 and 160 ms, respectively. For $[\text{Ca}^{2+}] = 2.0$ and $200 \mu\text{M}$ the distributions can be approximated by two exponential functions: a fast component with time constant 1-3 ms and a slow component with time constants 200 - 300 ms. The faster component (time constant ~ 2 ms) derives largely from immediate, ligand-independent transitions from the (110) state of the model to the active state, as set by the time constant $1/a_0$. The slower components derive from transitions involving the other 7 closed states, and are expected to be correspondingly complex. In practice, we are able to discern only a maximum of three-exponential functions by fitting to predicted closed time distributions.

The multi-exponential distributions of closed times lead to a 'burst-like' behaviour of channel gating. During bursts of rapid openings, short closings arise largely as any one of 3 active subunits undergoes round-trip transitions through the (110) states, whereas the more prolonged inter-burst intervals result from subunits entering longer lived inactive states that require ligand association or dissociation to return to the (110) state. A running average of instantaneous open probability P_o with a time window of 100 ms thus shows large fluctuations over time (Fig. 5B), similar to that observed experimentally [12].

Puff Latencies Following Steps of $[IP_3]$

In the present paper, we limit consideration of our IP_3R model to conditions where $[Ca^{2+}]$ is fixed at given values. The results are, therefore, not immediately applicable to cellular signaling, where cytosolic $[Ca^{2+}]$ fluctuates widely owing to Ca^{2+} flux through the IP_3R s themselves. An exception, however, concerns experimental observations of Ca^{2+} puffs evoked by flash photorelease of IP_3 , where the mean puff latency shortens with increasing $[IP_3]$ [7, 8]. In this case, the basal cytosolic $[Ca^{2+}]$ remains essentially unchanged before the puff, permitting us to simulate puff initiation by considering the stochastic variability in opening of an IP_3R channel following a step increase in $[IP_3]$ at constant $[Ca^{2+}]$. We assume that opening of a single IP_3R channel provides sufficient 'trigger' Ca^{2+} to activate neighboring channels and thereby evoke a puff [29], and estimate the number of IP_3R clustered at a puff site by fitting the stochastic simulation results to experimental data.

Responses of a single IP_3R channel to a step of $[IP_3]$

We first consider the latency of an individual channel following a step increase in IP_3 concentration. Initially, the channel is in equilibrium at biologically realistic resting conditions with cytosolic $[Ca^{2+}]_{Rest} = 0.1 \mu M$ and $[IP_3] = 0 \mu M$. At time $t = 0$, the concentration of IP_3 increases instantaneously from $0 \mu M$ to $[IP_3]_{Stim}$ to simulate the rapid photorelease of IP_3 by a UV flash. Examples of three responses to a step $[IP_3]_{Stim} = 10 \mu M$ are presented in Fig. 6A, illustrating the stochastic variability in channel kinetics. Here, we are concerned only with the latency to the first opening of the channel, and disregard subsequent openings. Fig. 6B and 6C plot distributions of channel first-opening latencies for various $[IP_3]_{Stim}$ and $[Ca^{2+}]_{Rest}$ obtained from the simulation and theory. The distributions follow skewed \cap -shaped curves that shift leftward and become narrower with increasing $[IP_3]_{Stim}$ (Fig. 6B) and $[Ca^{2+}]_{Rest}$ (Fig. 6C).

The mean first-opening latency of the channel as a function of $[IP_3]_{Stim}$ is shown in Fig. 7A for $[Ca^{2+}]_{Rest} = 0.1 \mu M$. The latency shortens markedly as $[IP_3]_{Stim}$ increases from 0 to 5 μM , but then reaches a minimum value of about 400 ms at higher $[IP_3]_{Stim}$. The mean first-opening latency of the channel as a function of $[Ca^{2+}]_{Rest}$ is shown in Fig. 7C for $[IP_3]_{Stim} = 0.1$ and 10 μM . An interesting observation is that changes in $[Ca^{2+}]_{Rest}$ from 0.05 to 0.2 μM cause an increase of the mean minimum latency at low $[IP_3]_{Stim}$ (from ~ 2500 to ~ 3500 ms for $[IP_3]_{Stim} = 0.1 \mu M$), but a decrease of the latency at high $[IP_3]_{Stim}$ (from ~ 650 to ~ 350 ms for $[IP_3]_{Stim} = 10 \mu M$).

These results can be understood in terms of the states of the IP_3R subunit model. For very small $[Ca^{2+}]_{Rest}$ ($\leq 0.01 \mu M$), more than 85% channel subunits are in the 000 state at $[IP_3] = 0 \mu M$. The binding of Ca^{2+} becomes rate-limiting, so that the latencies are long and have little dependence on $[IP_3]_{Stim}$. At physiological cytosolic $[Ca^{2+}]_{Rest}$ ($\sim 0.1 \mu M$), an important result is that a large proportion of subunits are predicated to be in a

Ca^{2+} -inhibited state (e.g. at $[\text{Ca}^{2+}] = 0.2 \mu\text{M}$ and $[\text{IP}_3] = 0 \mu\text{M}$, 75% of subunits are in the 001 or 011 states) before flash photo-release of IP_3 . As a result, changes in basal $[\text{Ca}^{2+}]_{\text{Rest}}$ will have dual opposing effects on the latency, with increasing $[\text{Ca}^{2+}]_{\text{Rest}}$ both increasing the steady-state probability of subunits being in Ca^{2+} -inhibited states, and yet also speeding the binding of Ca^{2+} to the activating site. At physiological cytosolic $[\text{Ca}^{2+}]_{\text{Rest}}$ our model shows that these two effects function differently at different $[\text{IP}_3]_{\text{Stim}}$. In detail, a 4-fold change in $[\text{Ca}^{2+}]_{\text{Rest}}$ from 0.05 to 0.2 μM results in a small shortening of the mean latency for large $[\text{IP}_3]_{\text{Stim}}$ and a small lengthening of the mean latency for small $[\text{IP}_3]_{\text{Stim}}$ (Fig. 7C).

Responses of clustered IP_3Rs to steps of $[\text{IP}_3]$

We next extend our simulation from a single IP_3R channel to a cluster of N functionally-independent channels representing a puff site. Again, the channels are equilibrated at the resting condition ($[\text{Ca}^{2+}]_{\text{Rest}} = 0.05 \mu\text{M}$ and $[\text{IP}_3] = 0 \mu\text{M}$), and a step of $[\text{IP}_3]$, i.e. $[\text{IP}_3]_{\text{Stim}}$, is imposed at time $t = 0$. We initially assume that opening of a single channel invariably triggers a puff by Ca^{2+} -induced Ca^{2+} release (CICR), so that the puff latency T_{Puff} is the interval from $t = 0$ until the first opening of any channel in the cluster. We then explore the effect of reducing the probability of puff initiation by opening of a single channel.

The mean puff latency T_{Puff} is plotted as a function of $[\text{IP}_3]_{\text{Stim}}$ and $[\text{Ca}^{2+}]_{\text{Rest}}$ in Figs. 7B & 7D, respectively, for clusters of $N = 50$ channels. In comparison with the first-opening latency of a single IP_3R , T_{Puff} is about 5 ~ 10 times shorter for a given $[\text{IP}_3]_{\text{Stim}}$ - as expected, since it represents the first among the 50 channels to open - but the general shape of the curve is similar.

An interesting observation is that the mean latency for clustered IP_3Rs for both large and small $[\text{IP}_3]_{\text{Stim}}$ at first shortens as $[\text{Ca}^{2+}]_{\text{Rest}}$ is raised from a low value (0.005 μM), but reaches a minimum at around 0.1 μM and thereafter actually shows a slight lengthening (Fig. 7D). An explanation is that binding of Ca^{2+} to activating sites is rate-limiting at very low $[\text{Ca}^{2+}]_{\text{Rest}}$, thus the latency first become shorter as $[\text{Ca}^{2+}]_{\text{Rest}}$ increases from 0.01 μM . But at higher concentrations ($>0.1 \mu\text{M}$) there is an increasing likelihood of subunits being in an inhibited state due to $K_4 = 0.072 \mu\text{M}$ (Fig. 1), so that the latency approaches a minimal value set by the dissociation rate b_2 from inhibitory Ca^{2+} binding sites.

Fig. 8A shows the puff latency distributions obtained from the theory and simulation for $[\text{IP}_3]_{\text{Stim}} = 10 \mu\text{M}$ and $[\text{Ca}^{2+}]_{\text{Rest}} = 0.1 \mu\text{M}$ considering clusters containing $N = 25, 50$ and 150 channels. The curves represent the stochastic variability in first-opening latencies and, since they reflect the population behavior of multiple channels, the

peaks of the distributions shift to shorter latencies with increasing N while the spread of the distribution narrows.

Number of IP₃Rs at a puff site

In order to compare model predictions with the experimental data, the mean puff latency T_{Puff} is re-plotted as a function of $1/[\text{IP}_3]_{\text{Stim}}$ in Fig. 8B for clusters of $N = 25, 50$ and 150 channels at $[\text{Ca}^{2+}]_{\text{Rest}} = 0.1 \mu\text{M}$, together with experimental data of puff latencies in *Xenopus* oocytes taken from [7, 8]. The experimental puff latency T_{Exp} can be fit as a linear function of $1/[\text{IP}_3]_{\text{Stim}}$ [7],

$$T_{\text{Exp}}(I_{\text{Stim}}) = T_0 + \frac{k}{I_{\text{Stim}}} \quad (11)$$

with the minimal latency $T_0 = 41 \text{ ms}$ and slope $k = 16.5 \text{ ms} \times \mu\text{M}$ (solid line in Fig. 8B). A good agreement with these experimental data was obtained by simulating a cluster containing 50 IP₃R channels.

In order to better quantify the agreement between model and experimental measurements of puff latencies (respectively, T_{Model} and T_{Exp}), we introduce an optimal matching function:

$$\Theta(N, [\text{Ca}^{2+}]_{\text{Rest}}) = -\lg(\Phi(N, [\text{Ca}^{2+}]_{\text{Rest}})) \quad (12)$$

with

$$\Phi = \frac{1}{M} \sum_{[\text{IP}_3]_{\text{Stim}}=I_1}^{I_M} \left(\frac{T_{\text{Model}}(N, [\text{IP}_3]_{\text{Stim}}) - T_{\text{Exp}}([\text{IP}_3]_{\text{Stim}})}{T_{\text{Exp}}([\text{IP}_3]_{\text{Stim}})} \right)^2 \quad (13)$$

A larger value of Θ indicates a better match between the modeled puff and the experimental observation.

The results are depicted graphically in Fig. 8C by contours of increasing Θ . Here we discuss the optimal function Θ by varying both the channel number N in the cluster and the resting Ca^{2+} concentration. The resting Ca^{2+} concentration in cytosol is about $0.05 \sim 0.2 \mu\text{M}$. An optimal region in N - $[\text{Ca}^{2+}]_{\text{Rest}}$ plane obtained with the model also centered at $[\text{Ca}^{2+}]_{\text{Rest}} = 0.12 \mu\text{M}$ with $N = 55$. Our simulation given in Fig. 8C suggests that the total channel number in a cluster may be in the range of $40 \sim 70$ (considering the contour of $\Theta = 2.0$ where $[\text{Ca}^{2+}]_{\text{Rest}}$ is in the biologically realistic range of $0.05 \sim 0.2 \mu\text{M}$).

Effect of reduced triggering probability on puff latency

In above discussion, the puff latency was calculated assuming that the first opening of any single channel in a cluster invariably trigger a puff by CICR. However, it is likely that brief channel openings may provide insufficient 'trigger' calcium to initiate a puff. We thus explored the effect of reducing the probability of puff initiation by reducing the probability P_{Trigger} that any given channel opening triggers a puff. Specifically, if the first

opening of a channel within a cluster failed to trigger a puff, we then checked whether the next opening event (of the same or a different channel) trigger a puff with the same P_{Trigger} , and so on until a puff was evoked.

Our simulation shows that the average puff latency varies only slightly as function of trigger probability P_{Trigger} for $P_{\text{Trigger}} \geq 30\%$. For example, the predicted cluster number N giving a good fit to the experimental data remained at about 50 for $P_{\text{Trigger}} > 50\%$; increasing to $N = 70$ for $P_{\text{Trigger}} = 30\%$ and $N = 100$ for $P_{\text{Trigger}} = 20\%$.

DISCUSSION

We propose a dynamic model of the type-1 IP₃ receptor in *Xenopus* oocytes, with the long-term goal of applying the model for stochastic simulations of cellular Ca²⁺ signaling dynamics within a realistic cytosolic environment. We specifically model the *Xenopus* oocyte system as this is subject of numerous cellular imaging studies [6-8, 29] and a wealth of data are available from patch-clamp data on oocyte nuclear IP₃R [9-12].

Our model assumes that each IP₃R channel is comprised from four identical and independent subunits. Like the De Young-Keizer model [14], each subunit consists of two independent Ca²⁺ binding sites - an activating and an inhibitory binding site - and one IP₃ binding site. Furthermore, we assume that a subunit becomes 'active' following a conformational change after both IP₃ binding sites and the activating, but not inhibitory, Ca²⁺ binding sites are occupied. The channel is open when at least three subunits are in the active state. The model provides a good fit to steady-state experimental data of channel open probability P_o [IP₃] [10, 11], though predicting a bell-shaped curve with [Ca²⁺] even at high concentrations of IP₃, different from the 'flat-topped' relationship obtained by Mak et al [11] and Baran [20]. Moreover, the model accounts well for the observed distributions of channel open and closed dwell times.

With the parameters given in Table 1, our model assumes that there is a negative allosteric interaction between the IP₃ site and the inhibitory Ca²⁺ site, i.e. IP₃ binding reduces the affinity of the inhibitory Ca²⁺ site (from K_4 to K_2), and Ca²⁺ binding to the inhibitory site decreases the affinity of the InsP₃ site (from K_1 to K_3). The affinity of the activating Ca²⁺ sites is independent of the inhibitory Ca²⁺ binding and IP₃ binding sites.

In the present paper we restrict consideration of the IP₃R model to situations where the Ca²⁺ concentration remains constant, and defer incorporating the effects of feedback by Ca²⁺ flux through the channel to future publications. Nevertheless, the results provide novel insights into the functioning of both individual IP₃Rs and the population behavior of clusters of IP₃Rs at puff sites.

Channel opening by 3 out of 4 subunits

As is the case for numerous ion channels, the IP₃R is multimer formed from several subunits. In some instances, exemplified by AMPA receptors [24], the single channel conductance increases in a stepwise fashion as more subunits become active following binding of ligand. However, the *Xenopus* oocyte IP₃R displays only a single major conductance level [11, 12], and our model correspondingly incorporates only a single open state. The question then arises as to how many of the four subunits must be active in order to open the channel.

We assume that the channel is open when either three or four subunits are in an 'active' state. This assumption has previously been applied in some IP₃R models [23], and we also assume there is only one conductance state irrespective of whether 3 or 4 subunits are active. An alternative approach to our simple model has been used in

allosteric modeling of the tetrameric IP₃ and ryanodine receptors [11, 30]; but such allosteric models are extremely complex by considering different conductance state with different open probability corresponding to different number of subunits in active state, which will involve numerous free parameters and be difficult to implement in stochastic simulations. The simulation shows that our simple IP₃R model can successfully reproduce two levels of experimental data obtained from patch-clamp of nuclear IP₃R and confocal imaging of clustered IP₃Rs.

One important consequence of assuming that channel openings occur with either 3 or 4 subunits in active state is that this model successfully predicts the dependence of open dwell time on ligand concentrations, whereas if the channel opening requires all 4 active subunits in active state, ligand-independent constant open dwell time would be expected since the open time depends only on the backward rate constant b_0 . The ligand-dependence of mean open time can be intuitively understood by distinguishing two types of channel open states – those involving only 3 active subunits (A3-only), and those involving 4 active subunits (A4-related). The mean dwell times in each state are relatively independent of ligand concentration, but A4-related openings are much longer than A3-only openings, since channel closure requires two subunits, rather than just one, to become inactive. Changes in mean channel open time thus derive from changes in the proportion of A3-only and A4-related openings. For example, at very low and very high $[Ca^{2+}]$ the probability of subunits becoming active is small, so almost all channel openings involve only 3 active subunits and the mean open time thus corresponds to the A3-only dwell time (~ 4 ms; Fig. 3B). Conversely, at optimal $[Ca^{2+}]$ one half of all openings are A4-related, so the channel open time is given by the average of the A3-only and A4-related dwell times (~ 9 ms).

The existence of distinct A3-only and A4-related openings may also explain experimental observations that the distributions of mean IP₃R channel open times follow two exponential components [12]. Mak et al. [12] proposed that these components arise from two kinetically distinguishable open states with different time constants, but our model suggests that they may instead reflect the different mean dwell times of A3-only and A4-related openings.

Furthermore, our model indicates a complex situation for the closed time distribution. In principle there are 486 distinct closed states and 9 distinct open states (Shuai, Parker & Pearson; unpublished), but in practice only two or three major exponential components can be discriminated from experimental or stochastic simulation data. The faster component primarily reflects brief closings caused by any one of the three active subunits undergoing multiple transitions between the active A-state and the inactive (110) state, whereas the slower components involve ligand binding transitions.

Inactivation of IP₃R at basal cytosolic $[Ca^{2+}]$

One feature of the model is that the dissociation constant of the inhibitory Ca^{2+} binding site increases enormously from $K_4 = 0.072 \mu\text{M}$ to $K_2 = 16 \mu\text{M}$ following binding of IP₃. This scheme is concordant with the conclusion of Mak et al [10] that the effect of IP₃ binding is not to directly activate the channel, as generally assumed, but rather to relieve

the channel from Ca^{2+} inhibition. A distinction, however is that whereas Mak et al [10] proposed that the sole action of IP_3 is to reduce the effective affinity of the inhibitory Ca^{2+} binding site, in our model it plays an additional role as an obligate agonist. That is to say, channel opening cannot occur in the absence of IP_3 even if the inhibitory Ca^{2+} sites are unoccupied and the activating sites bind Ca^{2+} [11].

An important consequence of the high affinity of the inhibitory Ca^{2+} binding in the absence of IP_3 is that a surprisingly high proportion of IP_3R are predicted to be in a Ca^{2+} -inhibited state under basal resting cytosolic conditions with zero $[\text{IP}_3]$. For example, with $[\text{Ca}^{2+}]_{\text{Rest}} = 0.1 \mu\text{M}$, about 60% of subunits would be Ca^{2+} -inhibited - resulting in about 82% of IP_3R having 2 or more subunits in an inhibited state so that the channel cannot immediately open on binding of IP_3 and activating Ca^{2+} . Thus, the latency of Ca^{2+} responses evoked by a step increase of $[\text{IP}_3]$ will depend strongly on the dissociation of Ca^{2+} from inhibitory sites, as well the rates of association of Ca^{2+} and IP_3 to activating sites. This is evident in Fig. 7C, where the mean first-opening latency of a single IP_3R initially shortens as $[\text{Ca}^{2+}]_{\text{Rest}}$ is raised from a low value ($0.005 \mu\text{M}$), but reaches a minimum at around $0.05 \mu\text{M}$ and thereafter actually shows a slight lengthening responding to $[\text{IP}_3]_{\text{Stim}} = 0.1 \mu\text{M}$. An explanation is that binding of Ca^{2+} to activating sites is rate-limiting at very low $[\text{Ca}^{2+}]_{\text{Rest}}$, but that at biological concentrations of $[\text{Ca}^{2+}]_{\text{Rest}}$ there is an increasing likelihood of subunits being in an inhibited state so that the latency approaches a minimal value set by the dissociation rate b_2 from inhibitory Ca^{2+} binding sites. Moreover, the magnitudes of Ca^{2+} release will depend on the available fraction of non-inactivated IP_3R , which in turn will be a function of the resting $[\text{Ca}^{2+}]$ prior to stimulation.

Number of IP_3R at a puff site

Finally, we extrapolated our model from the individual IP_3R to consider the latency of puffs generated by clusters containing multiple IP_3R . On the assumptions that IP_3R within a cluster are independent and that a puff is triggered by whichever channel in the cluster is the first to open, we obtained an optimal fit to experimental measurements of puff latency as a function of $[\text{IP}_3]$ [7, 8] for clusters containing $N = 40 - 70 \text{ IP}_3\text{Rs}$. This result is affected only slightly by changes of assumed resting Ca^{2+} concentration within a biologically-realistic range of 0.05 to $0.2 \mu\text{M}$.

The conclusion that clusters contain $40 - 70 \text{ IP}_3\text{Rs}$ likely represents a minimal estimate, since very brief channel openings may fail to initiate a puff, thereby requiring the number of IP_3R in the model cluster to be increased in order to then match the experimental data. However, this effect becomes appreciable only if the triggering probability is quite low. For example, our simulation shows that if channel openings have a 50% or better chance of initiating a puff ($P_{\text{Trigger}} > 50\%$), a cluster size with $N \sim 50$ still gives a good fitting to the experimental data of puff latency. At smaller P_{Trigger} , larger values of N are required to obtain a good fit to the experimental data; for example $N = 70$ for $P_{\text{Trigger}} = 30\%$. This treatment is simplified as compared to the biological situation, where calcium lingering from a channel opening that failed to trigger

a puff would likely increase the probability of a subsequent opening to trigger a puff. However, in our simulation, for simplicity, we assume that all the opening events for all the channels in the cluster has the same probability P_{Trigger} to trigger a puff; and that the resting calcium concentration is always fixed no matter how many opening channel failed to trigger a puff. We plan to address this question more fully in a future study by considering the stochastic dynamics of clustered channels, incorporating the feedback of released Ca^{2+} ions.

It should be noted that these values estimate the total number of IP_3R clustered at a puff site. In contrast, most experimental work has used measurements of puff amplitudes to estimate the number of open IP_3R channels that contribute to the Ca^{2+} flux during a puff. For example, we recently capitalized on the discovery of 'trigger' events that may represent the opening of a single IP_3R channel that initiates a puff [31] to construct a deterministic puff model that predicts the involvement of some 25 - 35 open channels [29]. Thus, it is likely that only a minority of IP_3R in a cluster open during a puff; as is expected if many receptors are inactivated at resting cytosolic $[\text{Ca}^{2+}]$ and Ca^{2+} dissociated from inhibitory binding sites only slowly on the timescale (a few hundred ms or shorter) of puff latencies.

Acknowledgements

This work was supported by NIH grants GM 65830 and GM48071.

REFERENCES

1. Berridge, M.J., P. Lipp, and M.D. Bootman. 2000. The versatility and universality of calcium signalling. *Nature Reviews Molecular Cell Biology*. 1: 11-21.
2. Taylor, C.W., P.C. da Fonseca, and E.P. Morris. 2004. IP₃ receptors: the search for structure. *Trends Biochem Sci*. 29: 210-9.
3. Bosanac, I., J.R. Alattia, T.K. Mal, J. Chan, S. Talarico, F.K. Tong, K.I. Tong, F. Yoshikawa, T. Furuichi, M. Iwai, T. Michikawa, K. Mikoshiba, and M. Ikura. 2002. Structure of the inositol 1,4,5-trisphosphate receptor binding core in complex with its ligand. *Nature*. 420: 696-700.
4. Bezprozvanny, I. 2005. The inositol 1,4,5-trisphosphate receptors. *Cell Calcium*. 38: 261-72.
5. Bezprozvanny, I., J. Watras, and B.E. Ehrlich. 1991. Bell-shaped calcium-response curves of Ins(1,4,5)P₃- and calcium-gated channels from endoplasmic reticulum of cerebellum. *Nature*. 351: 751-4.
6. Yao, Y., J. Choi, and I. Parker. 1995. Quantal Puffs of Intracellular Ca²⁺ Evoked by Inositol Trisphosphate in *Xenopus* Oocytes. *Journal of Physiology-London*. 482: 533-553.
7. Callamaras, N., J.S. Marchant, X.P. Sun, and I. Parker. 1998. Activation and coordination of InsP₃-mediated elementary Ca²⁺ events during global Ca²⁺ signals in *Xenopus* oocytes. *Journal of Physiology-London*. 509: 81-91.
8. Parker, I., Y. Yao, and V. Ilyin. 1996. Fast kinetics of calcium liberation induced in *Xenopus* oocytes by photoreleased inositol trisphosphate. *Biophysical Journal*. 70: 222-237.
9. Mak, D.O. and J.K. Foskett. 1994. Single-channel inositol 1,4,5-trisphosphate receptor currents revealed by patch clamp of isolated *Xenopus* oocyte nuclei. *J Biol Chem*. 269: 29375-8.
10. Mak, D.O., S. McBride, and J.K. Foskett. 1998. Inositol 1,4,5-trisphosphate activation of inositol trisphosphate receptor Ca²⁺ channel by ligand tuning of Ca²⁺ inhibition. *Proc Natl Acad Sci U S A*. 95: 15821-5.
11. Mak, D.O., S.M. McBride, and J.K. Foskett. 2003. Spontaneous channel activity of the inositol 1,4,5-trisphosphate (InsP₃) receptor (InsP₃R). Application of allosteric modeling to calcium and InsP₃ regulation of InsP₃R single-channel gating. *J Gen Physiol*. 122: 583-603.
12. Mak, D.O. and J.K. Foskett. 1997. Single-channel kinetics, inactivation, and spatial distribution of inositol trisphosphate (IP₃) receptors in *Xenopus* oocyte nucleus. *J Gen Physiol*. 109: 571-87.
13. Atri, A., J. Amundson, D. Clapham, and J. Sneyd. 1993. A Single-Pool Model for Intracellular Calcium Oscillations and Waves in the *Xenopus-Laevis* Oocyte. *Biophysical Journal*. 65: 1727-1739.
14. De Young, G.W. and J. Keizer. 1992. A single-pool inositol 1,4,5-trisphosphate-receptor-based model for agonist-stimulated oscillations in Ca²⁺ concentration. *Proc Natl Acad Sci U S A*. 89: 9895-9.
15. Kaftan, E.J., B.E. Ehrlich, and J. Watras. 1997. Inositol 1,4,5-trisphosphate (InsP₃) and calcium interact to increase the dynamic range of InsP₃ receptor-dependent calcium signaling. *J Gen Physiol*. 110: 529-38.

16. Sneyd, J. and J.F. Dufour. 2002. A dynamic model of the type-2 inositol trisphosphate receptor. *Proceedings of the National Academy of Sciences of the United States of America*. 99: 2398-2403.
17. Swillens, S., P. Champeil, L. Combettes, and G. Dupont. 1998. Stochastic simulation of a single inositol 1,4,5-trisphosphate-sensitive Ca^{2+} channel reveals repetitive openings during 'blip-like' Ca^{2+} transients. *Cell Calcium*. 23: 291-302.
18. Fraiman, D. and S.P. Dawson. 2004. A model of the IP_3 receptor with a luminal calcium binding site: stochastic simulations and analysis. *Cell Calcium*. 35: 403-413.
19. Sneyd, J. and M. Falcke. 2005. Models of the inositol trisphosphate receptor. *Progress in Biophysics & Molecular Biology*. 89: 207-245.
20. Baran, I. 2003. Integrated luminal and cytosolic aspects of the calcium release control. *Biophysical Journal*. 84: 1470-1485.
21. Hille, B., *Ion Channels of Excitable Membranes*. 2001: Sinauer Associates (3rd edition).
22. Adkins, C.E. and C.W. Taylor. 1999. Lateral inhibition of inositol 1,4,5-trisphosphate receptors by cytosolic Ca^{2+} . *Curr Biol*. 9: 1115-8.
23. Falcke, M., L. Tsimring, and H. Levine. 2000. Stochastic spreading of intracellular Ca^{2+} release. *Physical Review E*. 62: 2636-2643.
24. Rosenmund, C., Y. Stern-Bach, and C.F. Stevens. 1998. The tetrameric structure of a glutamate receptor channel. *Science*. 280: 1596-1599.
25. Bruno, W.J., J. Yang, and J.E. Pearson. 2005. Using independent open-to-closed transitions to simplify aggregated Markov models of ion channel gating kinetics. *Proceedings of the National Academy of Sciences of the United States of America*. 102: 6326-6331.
26. Yang J., W.B., WS Hlavacek, JE Pearson. 2006. On imposing detailed balance in complex reaction mechanisms *BIOPHYSICAL JOURNAL* 91: 1136-1141.
27. Shuai, J.W. and P. Jung. 2002. Stochastic properties of Ca^{2+} release of inositol 1,4,5-trisphosphate receptor clusters. *Biophysical Journal*. 83: 87-97.
28. Shuai, J.W. and P. Jung. 2003. Optimal ion channel clustering for intracellular calcium signaling. *Proc Natl Acad Sci U S A*. 100: 506-10.
29. Rose, H.J., S. Dargan, J. Shuai, and I. Parker. 2006. 'Trigger' events precede calcium puffs in *Xenopus* oocytes. *Biophys J*. 91: 4024-32.
30. Zahradnik, I., S. Gyorke, and A. Zahradnikova. 2005. Calcium activation of ryanodine receptor channels--reconciling RyR gating models with tetrameric channel structure. *J Gen Physiol*. 126: 515-27.
31. Shuai, J., H.J. Rose, and I. Parker. 2006. The Number and Spatial Distribution of IP_3 Receptors Underlying Calcium Puffs in *Xenopus* Oocytes. *Biophys J*. 91: 4033-44.

Table 1. The parameter values used in the IP₃R channel model.

	Parameter	Value (Unit)
Conformation Change Rate	a_0	540 s ⁻¹
	b_0	80 s ⁻¹
IP ₃ Binding Site	K_1	0.0036 μM
	a_1	60 $\mu\text{M}^{-1}\text{s}^{-1}$
	K_3	0.8 μM
	a_3	5.0 $\mu\text{M}^{-1}\text{s}^{-1}$
Activating Calcium Binding Site	K_5	0.8 μM
	a_5	150 $\mu\text{M}^{-1}\text{s}^{-1}$
Inhibitory Calcium Binding Site	K_2	16 μM
	a_2	0.2 $\mu\text{M}^{-1}\text{s}^{-1}$
	K_4	0.072 μM
	a_4	0.5 $\mu\text{M}^{-1}\text{s}^{-1}$

In the table, the disassociation constant $K_i = b_i / a_i$ with a_i on-binding rate and b_i off-binding rate. Due to the thermodynamic constraint, we have $K_1 K_2 = K_3 K_4$.

FIGURE LEGENDS

Fig. 1. Schematic diagram of the model of a single IP₃R channel subunit. Each subunit has an activation Ca²⁺ binding site, an inhibitory Ca²⁺ binding site, and an IP₃ binding site. We label the binding sites by the notation (*i j k*) where the index *i* represents the IP₃ binding site, *j* the activation Ca²⁺ binding site, and *k* the inhibitory Ca²⁺ binding site. The number 1 represents an occupied binding site and 0 a non-occupied site. Additionally we introduce a conformational change between 'active' and (A-state) and 'inactive' states (110) of the subunit. Values for the forward (*a*) and backward (*b*) rate constants associated with each transition are listed in Table 1. In the figure, *C* and *I* represent the concentrations of Ca²⁺ and IP₃, respectively. The bold arrows indicate the binding of ligands to different sites.

Fig. 2. Stochastic and deterministic modeling of IP₃R dynamics, and comparison with steady-state experimental data. (A) Example of stochastic simulation of IP₃R channel gating (upper panel), and the corresponding numbers of subunits in the active state (lower panel) at [IP₃] = 10 μM and [Ca²⁺] = 0.2 μM. Arrows mark openings that are associated with 4-related open states. (B) Graph shows the dependence of steady-state open probability (*P_o*) as a function of [Ca²⁺] for different concentrations of IP₃. Solid curves show results by the deterministic transition matrix theory. The results obtained by stochastic simulation are represented by open symbols (stars, [IP₃] = 10 μM; circles = 0.033 μM; squares = 0.02 μM; and triangles = 0.01 μM). Single-channel patch-clamp experimental data obtained from IP₃R on native nuclear membranes by Mak et al [10, 11] were re-plotted as filled symbols (stars [IP₃] = 10 μM; circles = 0.033 μM; squares = 0.02 μM; and triangles = 0.01 μM). (C,D) Mean open time *τ_o* (C) and the mean close time *τ_c* (D), respectively, as functions of [Ca²⁺] for different concentrations of IP₃ as indicated. Solid curves show results obtained with transition matrix theory, and open symbols show stochastic simulation results. Filled stars in (C) and (D) show corresponding experimental data at [IP₃] = 10 μM [10, 11].

Fig. 3. The dependence of *τ_o* on ligand concentration can be explained by a change in proportion of openings involving only three active subunits (A3-only openings) and those involving four active subunits (A4-related openings). (A) Stochastic simulation results demonstrating that the mean open times of A3-only and A4-related openings show only a slight dependence on [Ca²⁺] for [IP₃] = 10 μM. (B) The probabilities of A3-only and A4-related openings as functions of [Ca²⁺]. In both panels [IP₃] = 10 μM.

Fig. 4. Distributions of open times predicted by the IP₃R channel model. (A) Open time distributions for basal Ca²⁺ concentrations at [Ca²⁺] = 0.2, 2, and 50 μM with [IP₃] = 10 μM. Open symbols are results of stochastic simulations, and solid curves were obtained from the transition matrix theory. (B) Distributions of channel open durations involving A3-only and A4-related openings, derived from stochastic modeling at [Ca²⁺] = 0.12 μM and [IP₃] = 10 μM.

Fig. 5. Multi-component closed time distributions of the IP₃R channel result in 'burst-like' behavior. (A) Closed time distributions at $[Ca^{2+}] = 0.2, 2.0$ and $50 \mu M$ for $[IP_3] = 10 \mu M$. Open symbols are stochastic simulations and solid curves are from the transition matrix theory. (B) Two examples of the fluctuation in average channel open probability within a 100 ms running window, respectively for $[Ca^{2+}] = 0.1$ and $100 \mu M$ and $[IP_3] = 10 \mu M$.

Fig. 6. Distributions of first-opening latencies for a single IP₃R following different steps of $[IP_3]$ at various $[Ca^{2+}]$. (A) Three examples are shown of stochastic simulations for a step of $[IP_3]$ from 0 to $10 \mu M$ (lower panel) with $[Ca^{2+}] = 0.1 \mu M$. (B,C) Distributions of first-opening latencies following stepwise increases in $[IP_3]$ derived from stochastic modeling (open symbols) and theory (solid lines). Results are plotted for different magnitudes of $[IP_3]_{stim}$ with $[Ca^{2+}] = 0.1 \mu M$ (B), and for different $[Ca^{2+}]$ with $[IP_3]_{stim} = 10 \mu M$ (C).

Fig. 7. Mean first-opening latencies for single and multiple IP₃R following different steps of $[IP_3]_{stim}$ at various $[Ca^{2+}]$. (A, B) The mean first-opening latency of an individual IP₃R channel (A) as a function of $[IP_3]_{stim}$ with $[Ca^{2+}] = 0.1 \mu M$ and the corresponding latencies for the first opening of any channel among a population of 50 IP₃R channels (i.e. the predicted puff latency) (B). (C, D) Corresponding dependence of mean single-channel first-opening latency (C) and puff latency (D) for a cluster of 50 channels as functions of $[Ca^{2+}]$ for $[IP_3]_{stim} = 10 \mu M$ (stars) and $[IP_3]_{stim} = 0.1 \mu M$ (squares).

Fig. 8. Simulation and experimental measurements of puff latencies. (A) Predicted latency distribution of puffs for $[IP_3]_{stim} = 10 \mu M$ and $[Ca^{2+}]_{rest} = 0.1 \mu M$, assuming that a puff is evoked by the first opening of any IP₃R channel within clusters containing N IP₃Rs. The open symbols are for stochastic simulation results with $N = 25$ (down triangles), 50 (stars), or 150 (up triangles). The corresponding solid curves are obtained from the transition matrix theory. (B) Predicted mean puff latencies as functions of $[IP_3]_{stim}$ are shown for clusters containing $N = 25$ (down triangles), 50 (stars), and 150 (up triangles) channels, with $[Ca^{2+}]_{rest} = 0.1 \mu M$. For comparison, experimental data of puff latencies as a function of $[IP_3]$ step is re-plotted as filled squares from [7, 8] after normalizing as described in the text. (C) Goodness of fit of stochastic simulations to the experimental data as functions of both the number of IP₃R in a cluster and the resting Ca^{2+} concentration. Optimal agreement (maximal value of the index Θ) is obtained with $N \sim 40 - 70$ and $[Ca^{2+}]_{rest} \sim 0.05 - 0.2 \mu M$.

Fig.1

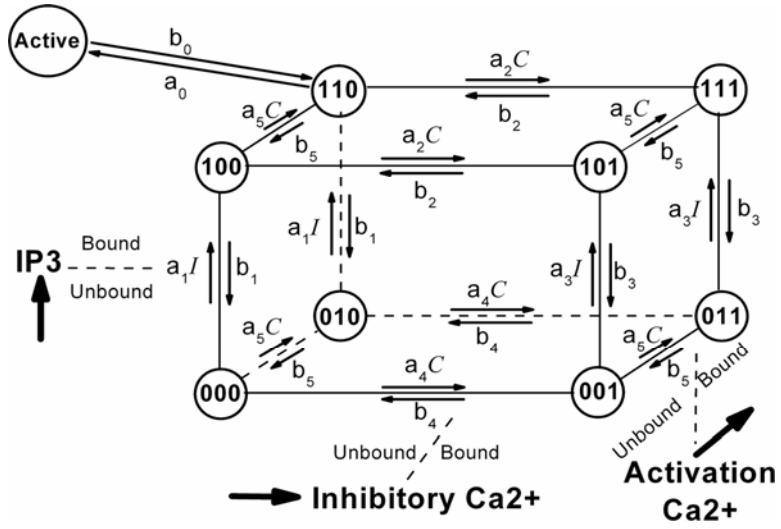


Fig.2

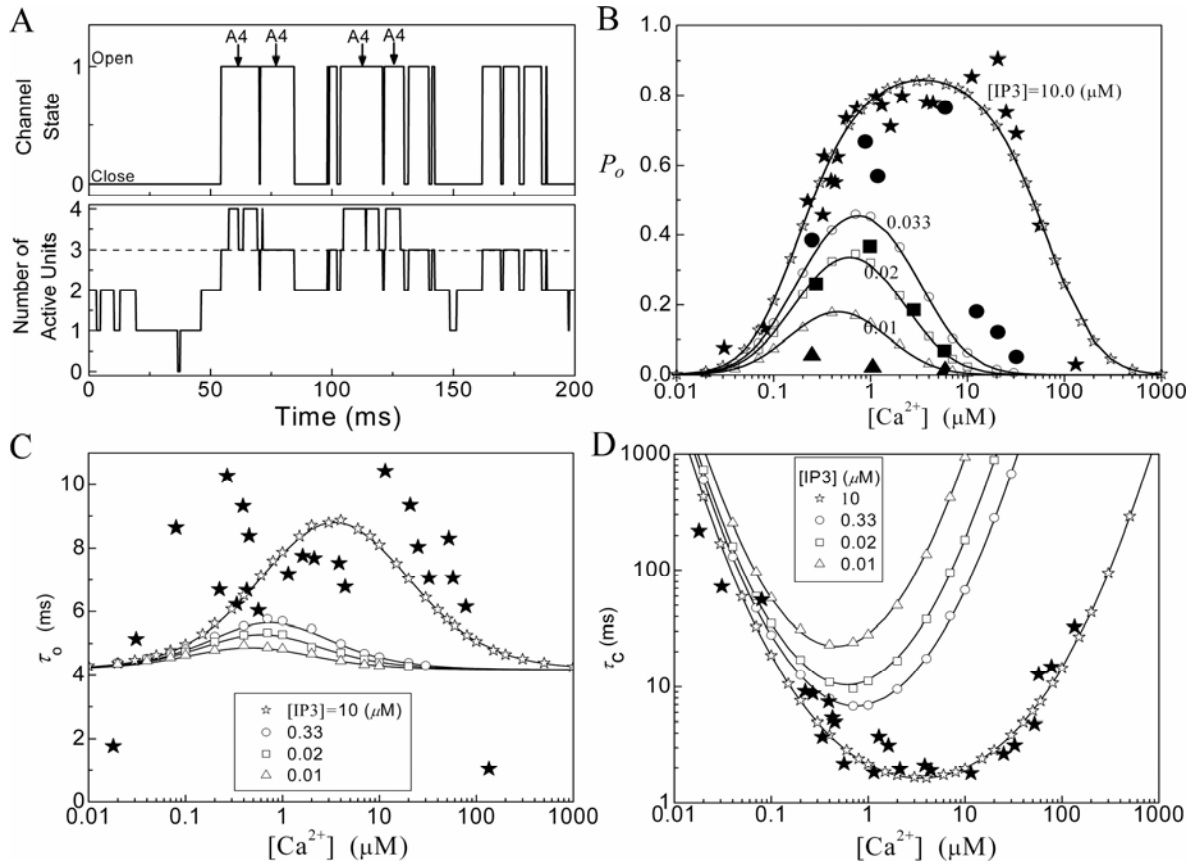


Fig.3

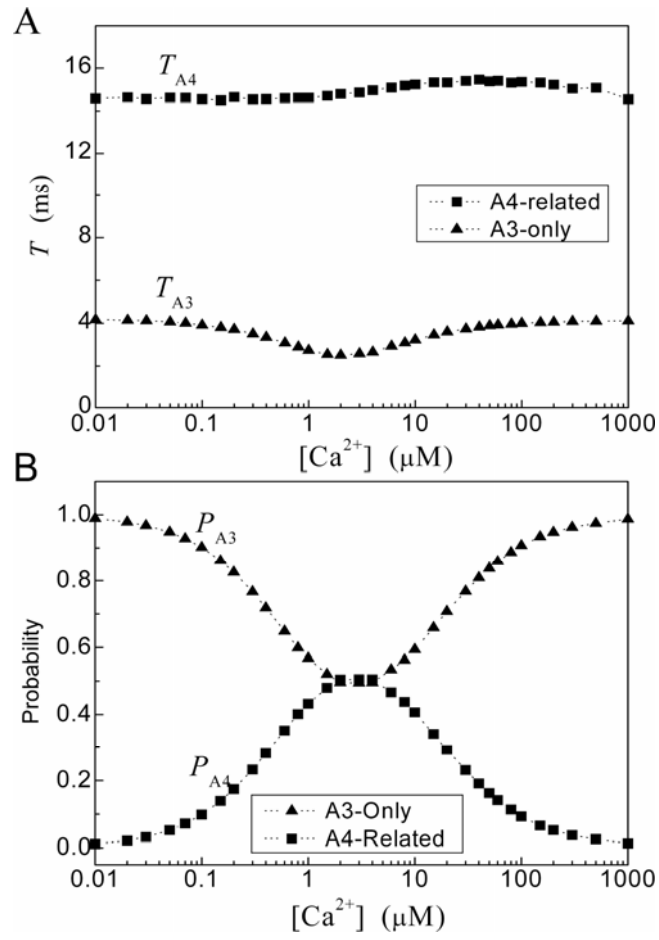


Fig.4

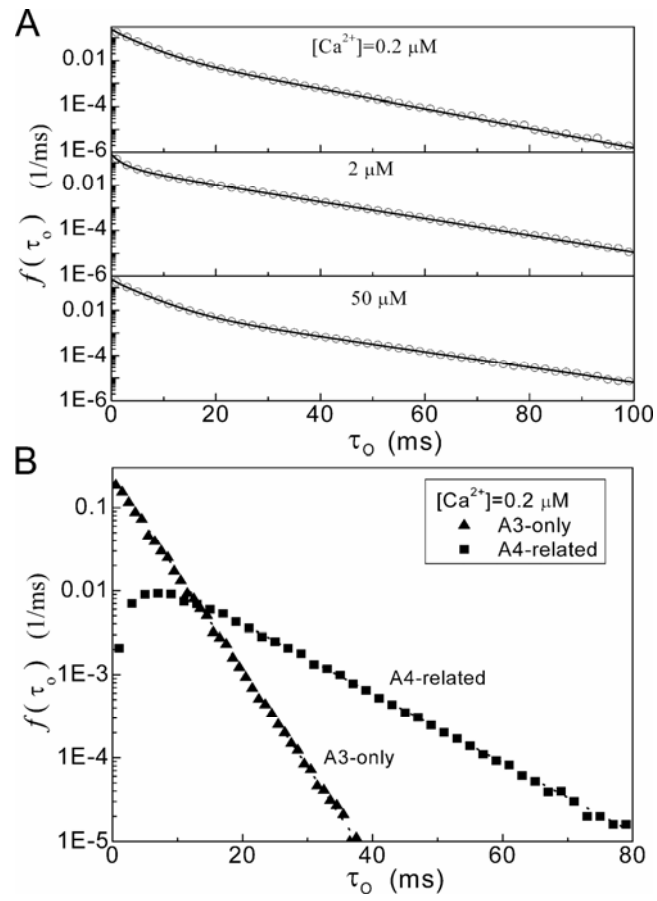


Fig.5

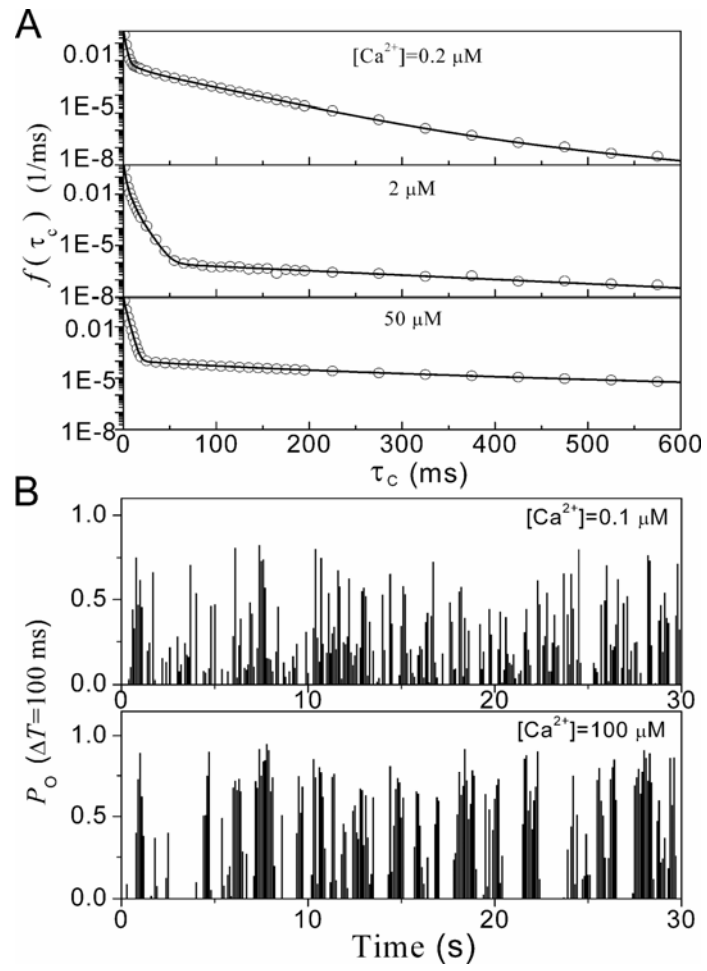


Fig.6

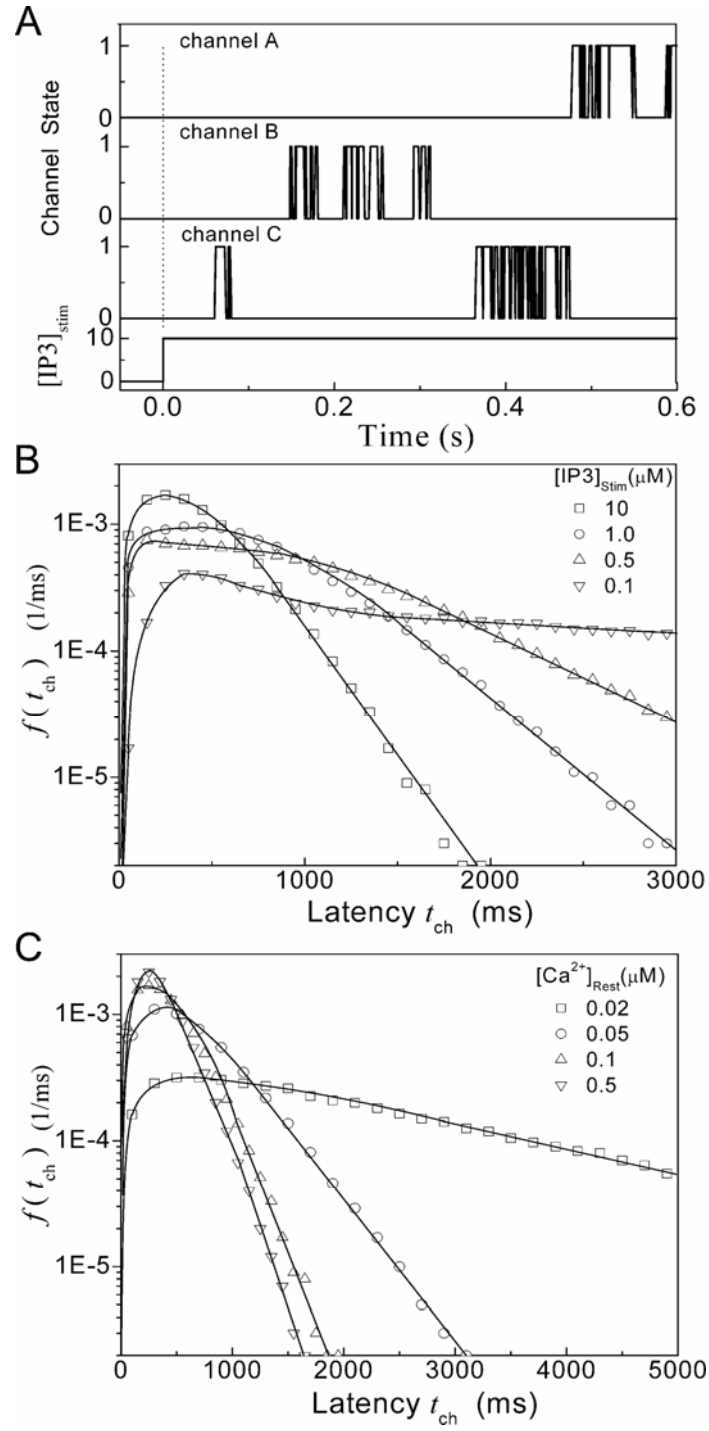


Fig.7

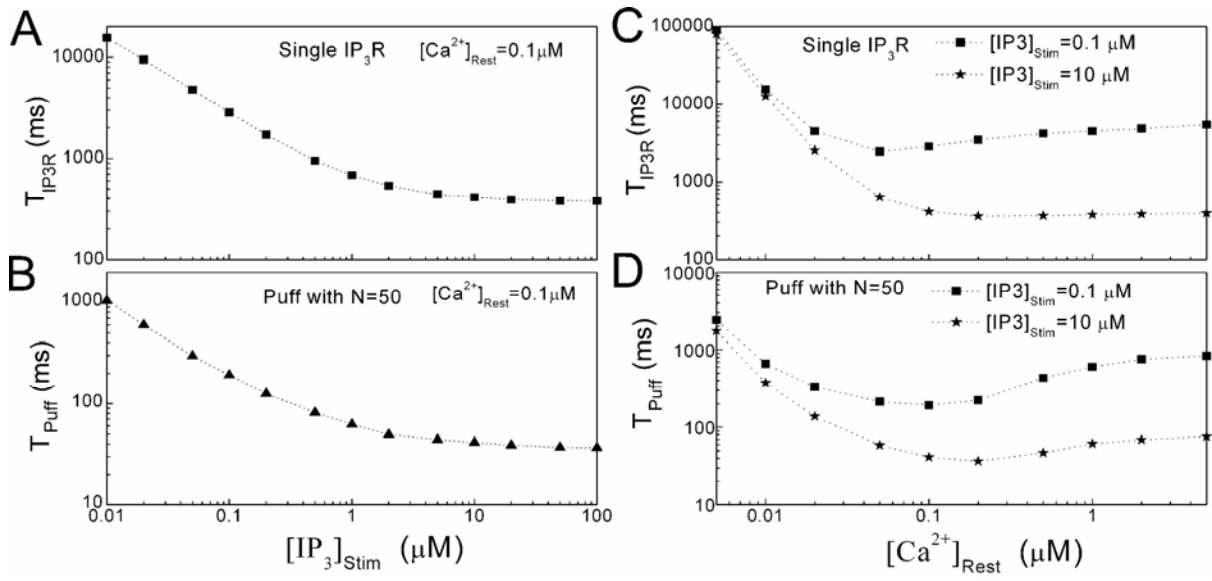


Fig.8

